Journal of The Electrochemical Society

OPEN ACCESS

Dysprosium and Gadolinium Double Doped Bismuth Oxide Electrolytes for Low Temperature Solid Oxide Fuel Cells

Dysprosium and Gadolinium Double Doped Bismuth Oxide Electrolytes for Low Temperature Solid Oxide Fuel Cells

Doh Won Jung,[a,=] Kang Taek Lee,[b,c,=,*] and Eric D. Wachsman[c,,z]**

[a] *Samsung Advanced Institute of Technology, Suwon-si 443-803, Korea*
[b] *Department of Energy Systems Engineering, DGIST, 50-1 Sang-Ri, Hyeonpung-Myeon, Dalseong-Gun, Daegu 711-873, Korea*
[c] *University of Maryland Energy Research Center, University of Maryland, College Park, Maryland 20742, USA*

Herein, we developed a novel double dopant bismuth oxide electrolyte system with dysprosium (Dy) and gadolinium (Gd). The effect of the co-dopants on phase stability and electrical properties was investigated. Phase transformation from cubic to rhombohedral was observed as Gd dopant concentration increased and consequently resulted in conductivity degradation. The stabilization of high temperature cubic phase was achieved with a total dopant concentration as low as ~12 mol% with 8 mol% Dy and 4 mol% Gd double dopant composition (8D4GSB) and this composition showed one of the highest total conductivity reported at this low temperature regime. In addition, the long-term stability of DGSB electrolytes was investigated.
 [DOI: 10.1149/2.0951605jes]

Manuscript submitted November 25, 2015; revised manuscript received January 29, 2016. Published February 9, 2016.

Over the last two decades, solid oxide fuel cell (SOFC) R&D has been concentrated on lowering the operating temperature (<700°C). It is because the operating temperature reduction can allow us to effectively reduce the system cost and increase the long-term stability of SOFCs.[1–3] Among SOFC electrolyte materials, yttria-stabilized zirconia (YSZ) system still remains the most popular choice due to its reasonably high ionic conductivity, especially at high temperature ~800°C, as well as high chemical and mechanical durability over 10,000 h.[4,5] At reduced operating temperatures, however, the ohmic polarization resistance of YSZ is exponentially increased due to its sluggish oxygen ion transport with the thermally activated nature.[2] Moreover, there has been repeatedly reported that YSZ materials show high reactivity with other high performance low temperature (LT)-SOFC components including doped ceria oxide electrolytes (e.g., Gd doped ceria) and cobaltite-based perovskite cathodes such as $La_{1-x}Sr_xCo_{1-y}Fe_yO_{3-\delta}$ or $Ba_{1-x}Sr_xCo_{1-y}Fe_yO_{3-\delta}$.[6] To address the issues of the conventional YSZ electrolytes, alternative superionic conductors with higher conductivities, such as doped ceria or stabilized bismuth oxides, have received attention to allow SOFC operation at reduced temperatures.[2]

Bismuth oxides in a fluorite structure (δ-Bi_2O_3) have been known for their highest oxygen ion conductivity among any reported SOFC electrolytes. This high ionic conductivity is attributed to their inherent defective structures with the intrinsic oxygen vacancy concentration of 25% as well as high anion mobility.[7] However, pure δ-Bi_2O_3 transforms to monoclinic α-phase on cooling below 730°C, resulting in a discontinuous drop in conductivity. Studies have shown that high temperature cubic phase of δ-Bi_2O_3 can be stabilized to room temperature by doping with a certain amount of other oxides. Therefore, numerous research efforts have been carried out to find optimal dopant and dopant concentration to achieve stabilized bismuth oxide with maximum ionic conductivity.

Verkerk et al. examined Dy_2O_3 doped Bi_2O_3 system and achieved face-centered cubic (fcc) structure with 28.5–50 mol% Dy_2O_3,[8] while Takahashi et al. investigated Gd_2O_3 doped Bi_2O_3 system and attained fcc structure with 35–50 mol% Gd_2O_3.[9] In both cases, a large amount of dopants were used to stabilize cubic structure. On the other hand, in our previous works of $(DyO_{1.5})_x(WO_3)_y(BiO_{1.5})_{1-x-y}$ (DWSB) and $(TbO_{1.75})_x(WO_3)_y(BiO_{1.5})_{1-x-y}$ (TWSB) electrolyte systems, it was found that the cubic phase-stabilization could be achieved with co-dopants at a relatively lower total dopant concentration (~12 mol%) compared to the single dopant system, resulting in higher conductivity.[10,11] In particular, the highest conductivity was obtained from $(DyO_{1.5})_{0.08}$-$(WO_3)_{0.04}$-$(BiO_{1.5})_{0.88}$ composition (8D4WSB) with the 12 mol% total dopant concentration.[12]

It is well known that the dopant ionic radius and polarizability affect the conductivity and stability of bismuth oxide-based electrolytes[13,14] and that for the lanthanide dopants investigated these two properties are linearly related.[14] For lanthanide dopants which stabilize the fcc structure of bismuth oxide, it was found that the anion ordering rate was slowest for Dy and fastest for Yb at 500°C since Dy^{3+} was the largest and most polarizable while Yb^{3+} was the smallest and least polarizable of the dopant cations within the fcc phase-stability window.[13,14] On the other hand, doping with larger-radii lanthanides such as Gd^{3+} resulted in formation of a rhombohedral phase.[9,13] However, co-doping changes the solid solubility range as compared with single dopant systems for cubic phase-stabilization (as demonstrated in the DWSB electrolyte system).[10]

In this work, we developed a Bi_2O_3-Dy_2O_3-Gd_2O_3 system (dysprosium- and gadolinium- stabilized bismuth oxide; DGSB) as LT-SOFC electrolytes. In order to achieve higher conductivity and improved stability with the desired cubic structure, the optimum composition with Dy and Gd dopants was systematically investigated via crystallographic analysis and electrochemical impedance spectroscopy (EIS). Further, the effect of dopant composition on the long-term stability and the structural evolution will be discussed.

Experimental

Sample preparation.—All samples were synthesized by the solid-state reaction of a stoichiometric mixture of Bi_2O_3 (99.9995% pure), Dy_2O_3 (99.99% pure), Gd_2O_3 (99.99% pure) from Alfa Aesar. First, various $(DyO_{1.5})_x(GdO_{1.5})_y(BiO_{1.5})_{1-x-y}$ compositions were prepared to find optimal dopant ratio and dopant concentration. Total dopant concentration was varied between 12 mol% and 18 mol%. $(DyO_{1.5})_{0.12-x}(GdO_{1.5})_x(BiO_{1.5})_{0.88}$ (where x = 0.04, 0.06, 0.08), $(DyO_{1.5})_{0.15-x}(GdO_{1.5})_x(BiO_{1.5})_{0.85}$ (where x = 0.05, 0.075, 0.10) and $(DyO_{1.5})_{0.12}(GdO_{1.5})_{0.06}(BiO_{1.5})_{0.82}$ were investigated. In this study, these compositions are referred to as 8D4GSB, 6D6GSB, 4D8GSB, 10D5GSB, 7.5D7.5GSB, 5D10GSB and 12D6GSB, respectively. Two step calcination was conducted with intermediate grinding of powders for DGSB electrolyte systems. Details on the electrolyte fabrication have been described in previous work.[10]

Characterization.—The crystallographic phase analysis of as-sintered and annealed samples was conducted by means of X-ray

=These authors contributed equally to this work.
*Electrochemical Society Member.
**Electrochemical Society Fellow.
zE-mail: ewach@umd.edu

diffraction analysis (XRD, Philips APD 3720). XRD pattern was obtained using CuKα radiation at room temperature between 20 to 80° (2θ). The total conductivity measurements were performed through two-point probe EIS using a Solartron 1260 over the frequency range of 0.1 Hz to 10 MHz. Due to the low impedance values of the bismuth oxide-based samples at high temperatures, a nulling technique was necessary to remove any artifacts caused by inductive responses of the test leads and the equipment. For that, the impedance of the lead wires without samples was measured and subtracted from the impedance with samples. The total conductivity was calculated between 300 and 700°C to obtain Arrhenius behavior. Each composition was annealed in air at 500°C for 100 h with EIS measured on an hourly basis to observe the long-term conductivity behavior as a function of time.

Results and Discussion

Phase stability.—In order to stabilize cubic bismuth oxides down to room temperature, dopants with smaller ionic radius than that of Bi^{3+} (1.17 Å for 6 coordination number) are usually used.[15] Jiang et al. found that with the same 25 mol% dopant content, cubic phase was obtained with Dy^{3+}, but Gd^{3+} resulted in rhombohedral phase.[13] In addition, Iwahara et al. demonstrated that depending on the dopant ionic radius of added oxides, Bi_2O_3-Ln_2O_3 (Ln = La – Yb) has rhombohedral phase for a relatively large ionic radius of Ln^{3+} and has fcc phase for a comparatively small radius of Ln^{3+}.[16] They also reported that Bi_2O_3-Ln_2O_3 could have mixed phases of fcc and rhombohedral with a cationic radius of medium size, depending on its composition[1,6]

These studies suggest that contraction of the highly defective δ-Bi_2O_3 structure is necessary to stabilize the high temperature bismuth phase down to room temperature. However, depending on the amount of contraction in structure, the stabilized bismuth could have cubic, rhombohedral, or mixed phases. We believe there exists a critical dopant ionic radius/composition relationship for cubic-phase stabilization, with relatively small radii Er^{3+} having the least dopant concentration (~15%) requirement among the lanthanides and the larger radii Dy^{3+} and Gd^{3+} having a larger concentration requirement, 28.5% and 35%, respectively.[13] Moreover, this relationship changes with double doping as cubic-phase stabilization can be achieved at a much lower total dopant concentration than with either of these dopants individually. Therefore, we investigated the optimal dopant composition, correct dopant ratio, and net concentration of Dy^{3+} and Gd^{3+} required to stabilize cubic bismuth oxides at total dopant concentrations significantly less than required for either of these lanthanides when individually substituted for Bi^{3+}.

In order to find the optimal dopant composition, various total dopant compositions of DGSB with three dopant content ratios of 2:1, 1:1 and 1:2 between Dy^{3+} and Gd^{3+} were prepared. Fig. 1 shows the XRD patterns of samples with total dopant concentration of 12 mol% including 8D4GSB, 6D6GSB and 4D8GSB, indicating there coexist both cubic and rhombohedral phases. The fraction of the rhombohedral phase (X_R) in the sample was estimated from XRD data using following equation.[17]

$$X_R = \frac{I^R_{(333)} + I^R_{(211)}}{I^C_{(111)} + I^R_{(333)} + I^R_{(211)}} \quad [1]$$

where I^C and I^R represent the intensities of the cubic and rhombohedral reflections, respectively. It was found that 8D4GSB has mainly cubic phase (89.4%) with minor rhombohedral phase (10.6%), while 6D6G and 4D8G exhibit large amounts of rhombohedral phase (68.8 and 87.17%, respectively) when a single calcination step was carried out.

These correspond to rhombohedral phases from $Bi_{0.775}Dy_{0.225}O_{1.5}$ and $Bi_{0.775}Gd_{0.225}O_{1.5}$.[18] This rhombohedral phase has a layered structure and $Bi_{0.775}Gd_{0.225}O_{1.5}$ has a slightly larger lattice parameter than $Bi_{0.775}Dy_{0.225}O_{1.5}$ due to the larger dopant size of Gd^{3+} compared with Dy^{3+}, while the peak positions of two rhombohedral phases are very similar. Analysis of XRD patterns show that the rhombohedral phase from DGSB compositions is attributed to $Bi_{0.775}Dy_{0.225}O_{1.5}$ or $Bi_{0.775}Gd_{0.225}O_{1.5}$. With the same total dopant concentration, the amount of rhombohedral phases increases as Gd concentration increases, indicating that the formation of rhombohedral phase is dependent on the amount of the larger radii Gd dopant. The ionic radius of Gd^{3+} is 1.078 Å, for 6-fold coordination, and that of Dy^{3+} is 1.052 Å[1,5]

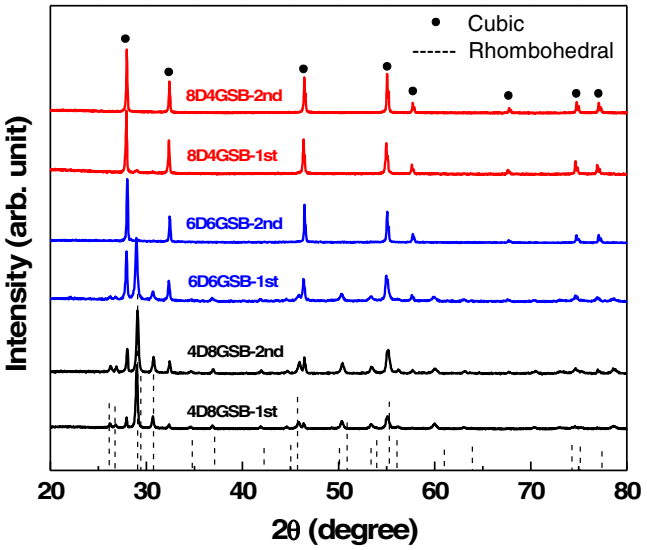

Figure 1. XRD patterns of 8D4GSB, 6D6GSB and 4D8GSB which were first calcined (1st) and second calcined (2nd) at 800°C for 16 h.

Additional calcination was carried out under the same conditions after intermediate grinding to ensure the phase of each composition. It was found that after the second calcination, a pure cubic phase was obtained for 8D4GSB as shown in Fig. 1. On the other hand, the other two compositions of 6D6GSB and 4D8GSB still had mixed phases, but with a greater amount of the cubic phase (i.e., 97.5 and 21.6%, respectively).

Fig. 2 shows the XRD patterns of three kinds of samples with 15 mol% total dopant concentration. The calculated fractions of the rhombohedral phase were 85.4, 96.0, and 95.46 for 10D5GSB, 7.5D7.5GSB and 5D10GSB, respectively, when a single calcination step was carried out. After the second calcination, the cubic phase in 10D5GSB was significantly increased (96.2%), while the rhombohe-

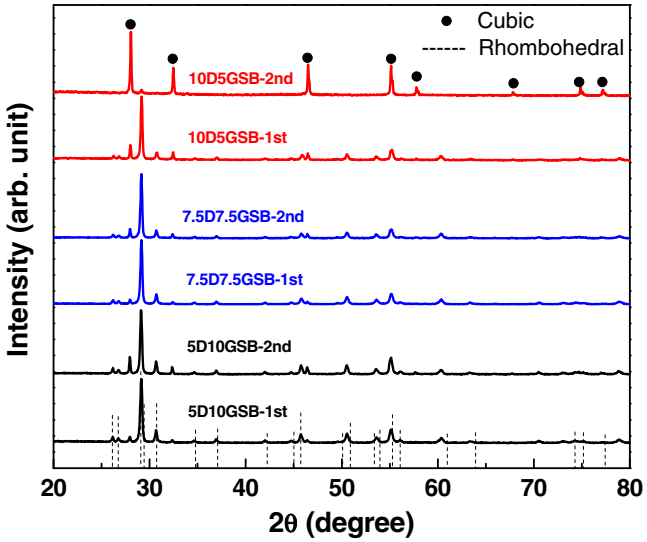

Figure 2. XRD patterns of 10D5GSB, 7.5D7.5GSB and 5D10GSB which was first calcined (1st) and second calcined (2nd) at 800°C for 16 h.

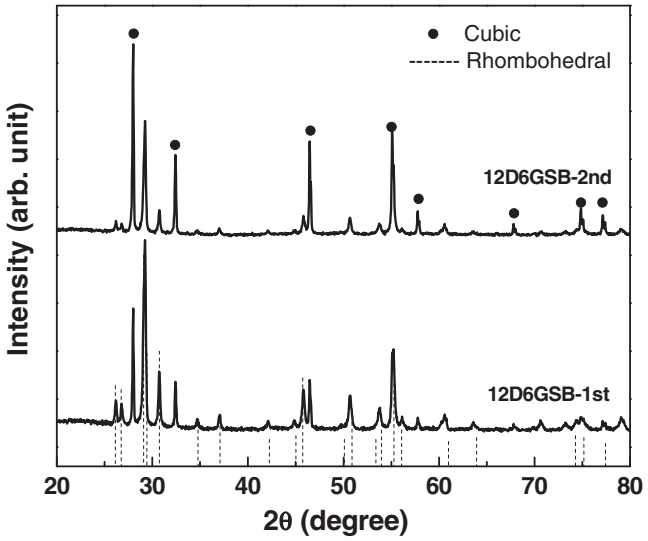

Figure 3. XRD patterns of 12D6GSB which was first calcined (1st) and second calcined (2nd) at 800°C for 16 h.

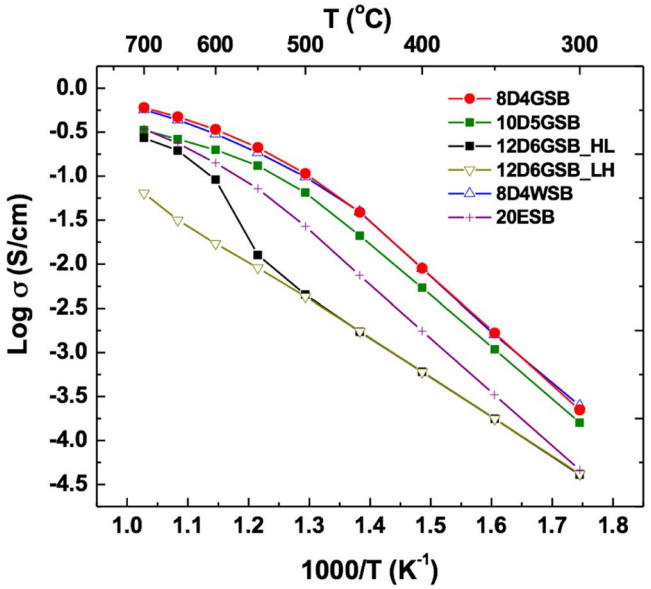

Figure 4. Arrhenius plot of conductivities for 8D4GSB, 10D5GSB, 12D6GSB, 8D4WSB[10] and 20ESB;[1] the conductivities were measured in both direction of temperature measurements, HL (High to Low) and LH (Low to High) for 12D6GSB.

dral phase was still dominant for 7.5D7.5GSB (91.4%) and 5D10GSB (86.73%).

Moreover, the lattice parameters of 8D4GSB and 10D5GSB after second calcination were estimated from the (111) peak position of XRD patterns (Fig. 2). The resultant values were 5.53 and 5.50 Å for 8D4GSB and 10D5GSB, respectively. Compared to the lattice parameter of pure δ-Bi_2O_3 (5.65 Å) reported by Yashima et al.,[19] this result clearly indicates that the higher total dopant concentration leads to greater lattice contraction of the co-doped bismuth oxide.

Lastly, 12D6GSB was prepared in the case of 18 mol% total dopant concentration based on phase observations from other compositions. However, 12D6GSB showed mixed cubic and rhombohedral phases even after second calcination step as shown in Fig. 3.

Based on the above results, it appears that the content of Dy_2O_3 should be larger than that of Gd_2O_3 within the limited total dopant concentration in order to achieve cubic-phase stabilization and high conductivity. Thus, we selected 8D4GSB (pure cubic), 10D5GSB (pure cubic) and 12D6GSB (cubic and rhombohedral mixture) for the conductivity measurements.

Conductivity.—Fig. 4 shows the Arrhenius behavior of the three DGSB compositions. The conductivity data of 20ESB and 8D4WSB were added for comparison purposes. It is clearly shown that the total conductivity of the DGSB electrolytes increases as the total dopant concentration decreases ($\sigma_{8D4GSB} > \sigma_{10D5GSB} > \sigma_{12D6GSB}$).

Moreover, the conductivity of 8D4GSB (e.g., 0.18 S/cm at 600°C) was comparable to that of 8D4WSB (e.g., 0.18 S/cm at 600°C), which is the highest conductivity composition reported in this temperature regime.[10] Both 8D4GSB and 10D5GSB have higher conductivity than that of 20ESB due to the lower total dopant concentration needed to stabilize the cubic phase with double dopants. As a result of the lower total dopant concentration there is less lattice strain effects so the conductivity approaches that of pure δ-Bi_2O_3 with double dopants.[10]

The highest total dopant composition, 12D6GSB, shows the lowest conductivity among the studied samples due to both its higher total dopant concentration and its mixed phase characteristics. It is worthwhile to note that the conductivity of 12D6GSB shows a discontinuity at around 550–600°C when the conductivity was measured from high to low temperature as shown in Fig. 4. This discontinuity is similar to a transition from the fcc phase to the monoclinic phase in pure Bi_2O_3. Fig. 5 shows the XRD pattern of 12D6GSB after conductivity measurement from high to low temperature. The result evidently shows that the majority of the cubic phase in 12D6GSB transformed into the rhombohedral phase. Thus, we believe that this discontinuity corresponds to the phase transition from the cubic to the rhombohedral phase. As shown in Fig. 3, it was not possible to achieve a pure fcc phase even after the second calcinations step. This implies that the fcc phase within 12D6GSB is only partially metastable and can easily transform to the lower conductivity rhombohedral phase with fast kinetics, thus showing a sharp drop in conductivity. Moreover, when conductivity of 12D6GSB was measured from low to high temperature it was found that a straight line without conductivity recovery was observed up to 700°C as shown in Fig. 4. This result is good in agreement with the previous report that the rhombohedral phase is relaxed to the high temperature cubic phase above 700°C.[20]

Long-term stability.—The long-term stability tests were performed for these 8D4GSB, 10D5GSB and 12D6GSB compositions at 500°C for 100 h and the results are plotted as a function of time in

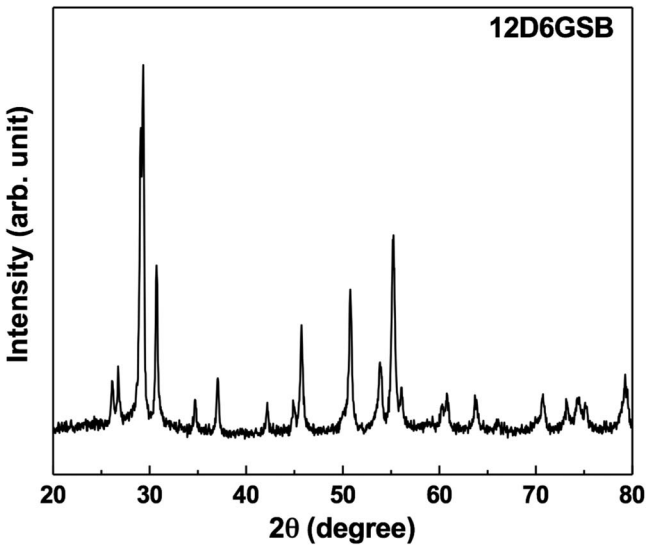

Figure 5. XRD pattern of 12D6GSB after conductivity measurement from high to low temperature in Fig. 4.

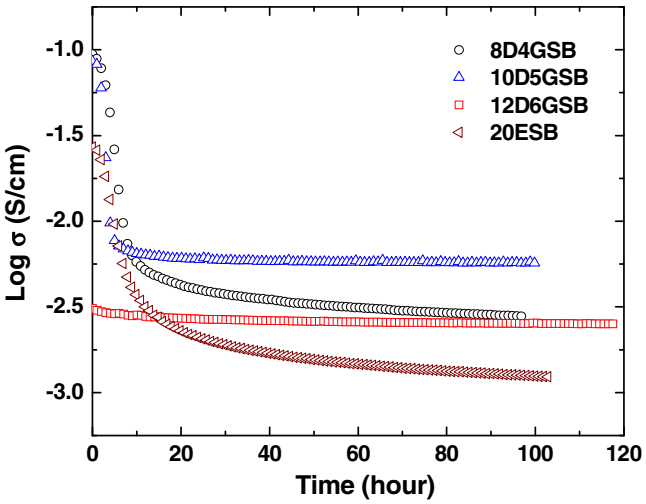

Figure 6. Conductivity vs. time for 8D4GSB, 10D5GSB and 12D6GSB annealed at 500°C; 20ESB is added for comparison.[1]

Fig. 6. For all samples, long-term stability tests were conducted after the initial conductivity measurement from 700 to 300°C. 8D4GSB and 10D5GSB underwent an initial large conductivity degradation and then reached a plateau. This conductivity degradation behavior is very similar to that of 20ESB. On the other hand, the conductivity of 12D6GSB maintained the initial conductivity for 100 h, albeit with an initial conductivity that was much lower than that of others. This suggests that the cubic to rhombohedral phase change of 12D6GSB was almost complete during initial conductivity measurements and that no conductivity degradation is observed after the phase transformation is complete. Jiang et al. also observed that $(Bi_2O_3)_{0.75}(Ln_2O_3)_{0.25}$ (Ln = La, Nd, Sm) had a rhombohedral phase and exhibited only very small decay during annealing at 500°C.[21]

Fig. 7 shows XRD patterns of 8D4GSB and 10D5GSB before and after annealing at 500°C. Even though both compositions experienced similar conductivity degradation trends with time, XRD results were quite different. 8D4GSB maintained the cubic phase, while 10D5GSB underwent a complete transformation from the cubic to rhombohedral phase after only 24 h annealing at 500°C as shown in Fig. 7b.

This result implies that the conductivity degradation of 8D4GSB at 500°C is attributed to occupancy ordering and positional ordering mechanisms without phase transformation.[22,23] This could be explained from the initial phase stability analysis as shown in Figs. 1 and 2. After first calcination step 8D4GSB had almost cubic phase, while 10D5GSB had larger amount of rhombohedral phase. Therefore, the fcc phase of 10D5GSB is more metastable than that of 8D4GSB, thus having a much faster kinetic rate of phase transformation to the rhombohedral phase at 500°C.

In Fig. 6 and Fig. 7, it is noteworthy that after the rhombohedral phase is formed, no conductivity degradation was observed with 10D5GSB. This observation suggests that the rhombohedral phase with the layered structure may not experience anion ordering due to the lower symmetry.

Conclusions

In this study we developed a new co-dopant (Dy and Gd) stabilized bismuth oxide system. The phase pure bismuth oxide with a cubic crystal structure was achieved with a total dopant concentration as low as ~12 mol% with 8 mol% Dy and 4 mol% Gd double dopant composition (8D4GSB), while we observed a tendency to form a rhombohedral phase as the amount of Gd dopant or total dopant concentration increased. Among tested compositions, 8D4GSB showed the highest total conductivity, which is one of the highest conductivities ever reported at the temperature range from 300 to 700°C.

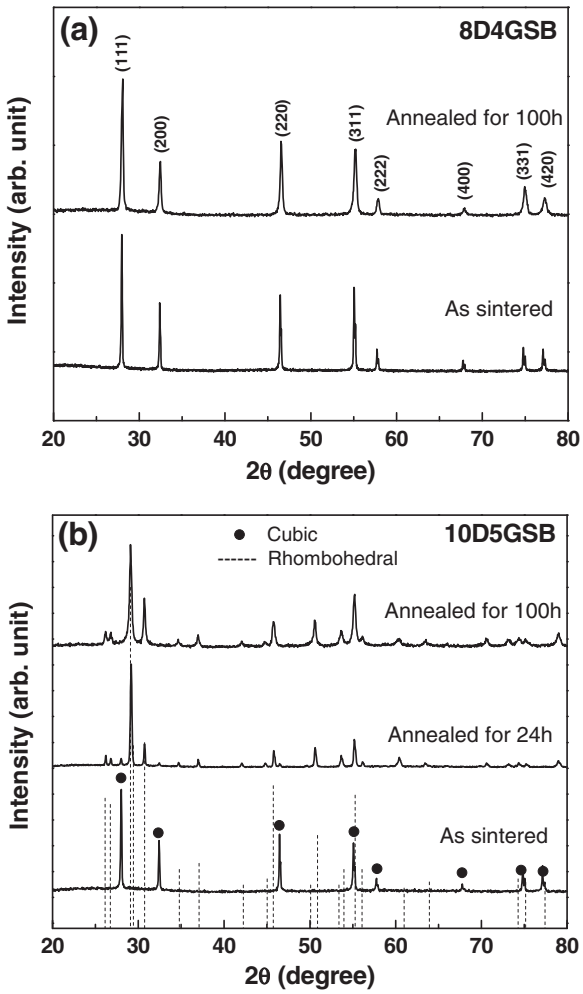

Figure 7. XRD patterns of (a) 8D4GSB and (b) 10D5GSB which was as-sintered and annealed at 500°C for 24 h and 100 h.

During long-term stability tests, 8D4GSB underwent conductivity degradation due to anion ordering, while 10D5GSB and 12D6GSB showed conductivity degradation resulting from a cubic to rhombohedral phase transformation at ~500°C.

Acknowledgments

E. D. Wachsman acknowledges support of Redox Power Systems and K. T. Lee acknowledges support of Basic Science Research Program through the National Research Foundation of Korea (NRF) funded by the Ministry of Education (2014R1A1A2057681).

References

1. E. D. Wachsman and K. T. Lee, *Science*, **334**, 935 (2011).
2. K. T. Lee, H. S. Yoon, and E. D. Wachsman, *Journal of Materials Research*, **27**, 2063 (2012).
3. K. T. Lee and E. D. Wachsman, *MRS Bulletin*, **39**, 783 (2014).
4. N. Q. Minh, *Journal of the American Ceramic Society*, **76**, 563 (1993).
5. B. C. H. Steele and A. Heinzel, *Nature*, **414**, 345 (2001).
6. W. S. Jang, S. H. Hyun, and S. G. Kim, *Journal of Materials Science*, **37**, 2535 (2002).
7. E. D. Wachsman, *Journal of the European Ceramic Society*, **24**, 1281 (2004).
8. M. J. Verkerk and A. J. Burggraaf, *Journal of the Electrochemical Society*, **128**, 75 (1981).
9. T. Takahashi, T. Esaka, and H. Iwahara, *Journal of Applied Electrochemistry*, **5**, 197 (1975).
10. D. W. Jung, K. L. Duncan, and E. D. Wachsman, *Acta Materialia*, **58**, 355 (2010).
11. D. W. Jung, K. T. Lee, and E. D. Wachsman, *Journal of the Korean Ceramic Society*, **51**, 260 (2014).

12. D. W. Jung, K. L. Duncan, M. A. Camaratta, K. T. Lee, J. C. Nino, and E. D. Wachsman, *Journal of the American Ceramic Society*, **93**, 1384 (2010).
13. N. Jiang and E. D. Wachsman, *J Am Ceram Soc*, **82**, 3057 (1999).
14. E. D. Wachsman, S. Boyapati, and N. Jiang, *Ionics*, **7**, 1 (2001).
15. R. D. Shannon, *Acta Crystallographica, Section A*, **A32**, 751 (1976).
16. H. Iwahara, T. Esaka, T. Sato, and T. Takahashi, *J Solid State Chem*, **39**, 173 (1981).
17. K. Z. Fung and A. V. Virkar, *Journal of the American Ceramic Society*, **74**, 1970 (1991).
18. M. Drache, S. Obbade, J. P. Wignacourt, and P. Conflant, *J Solid State Chem*, **142**, 349 (1999).
19. M. Yashima, D. Ishimura, and K. Ohoyama, *Journal of the American Ceramic Society*, **88**, 2332 (2005).
20. A. Watanabe and T. Kikuchi, *Solid State Ionics*, **21**, 287 (1986).
21. N. Jiang, Stanford University, CA, 1994.
22. S. Boyapati, E. D. Wachsman, and N. X. Jiang, *Solid State Ionics*, **140**, 149 (2001).
23. S. Boyapati, E. D. Wachsman, and B. C. Chakoumakos, *Solid State Ionics*, **138**, 293 (2001).